Rotational spectra of the van der Waals complexes of molecular hydrogen and OCS

Zhenhong Yu, Kelly J. Higgins, and William Klemperer
Department of Chemistry and Chemical Biology, Harvard University, Cambridge, Massachusetts 02138, USA

Michael C. McCarthy and Patrick Thaddeus
Harvard-Smithsonian Center for Astrophysics, Cambridge, Massachusetts 02138, USA and Division of Engineering and Applied Sciences, Harvard University, Cambridge, Massachusetts 02138, USA

Kristine Liao and Wolfgang Jäger
Department of Chemistry, University of Alberta, Edmonton, Alberta T6G 2G2, Canada

(Received 11 May 2007; accepted 15 June 2007; published online 3 August 2007)

The *a*- and *b*-type rotational transitions of the weakly bound complexes formed by molecular hydrogen and OCS, para-H_2–OCS, ortho-H_2–OCS, HD–OCS, para-D_2–OCS, and ortho-D_2–OCS, have been measured by Fourier transform microwave spectroscopy. All five species have ground rotational states with total rotational angular momentum $J=0$, regardless of whether the hydrogen rotational angular momentum is $j=0$ as in para-H_2, ortho-D_2, and HD or $j=1$ as in ortho-H_2 and para-D_2. This indicates quenching of the hydrogen angular momentum for the ortho-H_2 and para-D_2 species by the anisotropy of the intermolecular potential. The ground states of these complexes are slightly asymmetric prolate tops, with the hydrogen center of mass located on the side of the OCS, giving a planar T-shaped molecular geometry. The hydrogen spatial distribution is spherical in the three $j=0$ species, while it is bilobal and oriented nearly parallel to the OCS in the ground state of the two $j=1$ species. The $j=1$ species show strong Coriolis coupling with unobserved low-lying excited states. The abundance of para-H_2–OCS relative to ortho-H_2–OCS increases exponentially with *decreasing* normal H_2 component in H_2/He gas mixtures, making the observation of para-H_2–OCS in the presence of the more strongly bound ortho-H_2–OCS dependent on using *lower* concentrations of H_2. The determined rotational constants are $A=22\,401.889(4)$ MHz, $B=5993.774(2)$ MHz, and $C=4602.038(2)$ MHz for para-H_2–OCS; $A=22\,942.218(6)$ MHz, $B=5675.156(7)$ MHz, and $C=4542.960(7)$ MHz for ortho-H_2–OCS; $A=15\,970.010(3)$ MHz, $B=5847.595(1)$ MHz, and $C=4177.699(1)$ MHz for HD–OCS; $A=12\,829.2875(9)$ MHz, $B=5671.3573(7)$ MHz, and $C=3846.7041(6)$ MHz for ortho-D_2–OCS; and $A=13\,046.800(3)$ MHz, $B=5454.612(2)$ MHz, and $C=3834.590(2)$ MHz for para-D_2–OCS. © *2007 American Institute of Physics*. [DOI: 10.1063/1.2756534]

I. INTRODUCTION

Clusters of molecular hydrogen have attracted extensive theoretical and experimental attention since Grebenev *et al.* reported the first observation of the unique quantum phenomenon of molecular superfluidity from para-H_2 (p-H_2) clusters[1–3] using carbonyl sulfide (OCS) as a molecular probe embedded inside the clusters. The weakly bound $(p\text{-}H_2)_n$–OCS clusters are formed inside a helium droplet using the experimental technique developed by Toennies and co-workers[4–6] and Scoles and co-workers.[7,8] At $n=6$, the pronounced *Q* branch of the C–O stretching mode disappears. They suggest that this absence of angular momentum along the inertial *a* axis provides the physical evidence for the existence of p-H_2 superfluidity. This method overcomes the solidification of bulk hydrogen at these temperatures (0.37 K for ^{4}He and 0.15 K for mixed ^{4}He/^{3}He droplets). Although a detailed understanding of this apparent superfluidity is not complete, most studies attribute it to the high permutation exchange symmetry of para-H_2.[9,10] In a particularly elegant study of HCN–$(HD)_n$ in helium droplets, Moore and Miller employed strong electric fields to quench the rotation of the cluster and to facilitate the identification of *n*, followed by the observation of the rotational transitions of HCN–$(HD)_n$ at a zero applied field. They observed a similar free rotation of the probed molecule HCN at $n=12$[11] and suggested that it might have arisen from a significant increase in the anisotropy of the solvent environment. The thorough experimental and theoretical investigation of the intermolecular interaction between hydrogen and OCS as well as its isotopic dependence should be very helpful in understanding this unique phenomenon. An early theoretical study showed that the anisotropy of the interaction potential may play an important role.[12]

Weakly bound hydrogen complexes distinguish themselves from other binary van der Waals complexes by the large amplitude intermolecular motions and different bound states formed by species with different nuclear spin states: para-H_2 (p-H_2, with $I=0$) and ortho-H_2 (o-H_2, $I=1$) or ortho-

D_2 (o-D_2, $I=0$ and 2) and para-D_2 (p-D_2, $I=1$), where I is the nuclear spin angular momentum. Using j to denote the hydrogen rotational angular momentum, only even j rotational levels are allowed for species with $I=0$ or 2 and only odd j levels are allowed for species with $I=1$, while all j levels are allowed for HD. The large rotational constant of hydrogen (30–60 cm^{-1}) and the extremely low ($T_{rot} \sim 1$ K) rotational temperature of a supersonic beam ensure that the hydrogen in the beam and in complexes formed in the beam are in their lowest allowed rotational state, either $j=0$ or 1 based on nuclear spin statistics. The nuclear spin conversion of symmetrical hydrides is an extremely slow process because it requires both nuclear spin angular momentum and rotational angular momentum to be changed simultaneously. It is particularly difficult for H_2 and D_2,[13] leading to five distinct hydrogen-OCS complexes formed from each of the two spin states of H_2 and D_2, plus HD.

In addition to the spin restrictions on the allowed rotational levels, the symmetry of the intermolecular potential dictates that mixing between hydrogen rotational levels in hydrogen-OCS complexes is restricted to either all even or all odd j levels. Unless the anisotropy of the intermolecular potential with respect to hydrogen rotation is large compared to the allowed $\Delta j=2$ rotational excitations, mixing of different rotational levels of hydrogen with the same parity will be small. Thus, j has generally been considered as a good quantum number,[14] and the rotational spectra of these complexes should be simple compared to those of the other weakly bound complexes with more hindered internal rotation. The hydrogen spatial distribution in complexes with $j=0$ will be quite close to spherical, and the hydrogen in these species can be treated approximately as an atom, so that the rotational energy levels will be similar to those of a semirigid asymmetric top such as He–OCS. A previous study of hydrogen-OCS complexes estimated the character of the hydrogen spatial distribution to be more than 98% $j=0$ for p-H_2–OCS, HD–OCS, and o-D_2–OCS (Ref. 15) based on the analysis of the nuclear hyperfine structure of the hydrogen submolecule.

For complexes with $j=1$, the situation is more complicated. Although mixing of higher j states will be small due to the larger $j=1-3$ energy gap, the presence of three components of $j=1$ hydrogen gives rise to three "orientational" states of the complex. In the limit of zero anisotropy and neglecting Coriolis contributions, the three states will be degenerate. Weak anisotropy in the potential reduces the degeneracy but retains the three orientational states to an extent dictated by the intermolecular potential and the location of the hydrogen center of mass relative to the (linear) molecule. Hydrogen-OCS complexes, which are planar with the hydrogen located on the side of the OCS,[16,17] belong to the C_s point group, whose symmetry elements are the identity and the reflection plane. This group has only two one-dimensional irreducible representations. With the z axis perpendicular to the reflection plane, the $m_j=0$ component of $j=1$, $\cos\theta$, transforms like the A'' representation, while the two $|m_j|=1$ components, $\sin\theta\exp(\pm i\varphi)$, transform like the A' in-plane representation. We use a Cartesian basis in which the A'' component, p_z, remains the same but the two orthogonal A' components, p_x and p_y, are $\sin\theta\cos\varphi$ and $\sin\theta\sin\varphi$, respectively.

The intermolecular potential shifts and mixes the $j=1$ components to first order through matrix elements of the form $\langle jm_\alpha|V_{int}|jm_{\alpha'}\rangle$. The potential transforms as the A' representation, and thus the only nonzero matrix elements are the three diagonal elements and the off-diagonal elements that connect the two A' components p_x and p_y. The energy matrix of the $j=1$ triplet is reduced to a one-dimensional (A'') and a two-dimensional (A') set. We find from a computed potential[16] that, in order of increasing energy, the levels are A' with the hydrogen aligned nearly parallel to the OCS axis, A'' with the hydrogen perpendicular to the reflection plane, and the highest A' with the hydrogen aligned nearly perpendicular to the OCS axis. The out-of-plane A'' orientational state is the only low energy intermolecular level of that symmetry and, together with the excited in-plane A' state, gives the $j=1$ species two additional low-lying states to go with the in-plane van der Waals bending and stretching states that exist for both the $j=0$ and 1 species. As will be discussed later, these extra states complicate the spectra of the $j=1$ species through Coriolis interactions with the ground state. Thus, the threefold degeneracy of the $j=1$ components is completely removed, or, equivalently, the angular momentum is quenched. It is useful to distinguish the magnitude of the angular momentum from the vector angular momentum, so that although the vector angular momentum is quenched, the magnitude of the hydrogen angular momentum, j, remains a quite good quantum number.

High-resolution infrared spectra for all forms of the hydrogen-OCS complex have been reported by Tang and McKellar.[17] These complexes, like He–OCS, are slightly asymmetric prolate rotors in the ground state. Since the vibrational transition moment is along the OCS and thus close to the a axis of the complex (Fig. 1), b-type transitions proved difficult to detect in their study and thus only a-type rovibrational transitions of the C–O stretching mode were measured. b-type transitions, however, are particularly useful in determining the ground state structure and its variation with hydrogen unit, and thus one of the goals of the current study was to measure b-type rotational transitions. In conjunction with the experimental work reported here, we have calculated a high-level four-dimensional *ab initio* intermolecular potential for hydrogen-OCS, the details of which have been presented elsewhere.[16] Subsequently, Paesani and Whaley reported a similar *ab initio* potential, but with the inclusion of the explicit dependence on the Q_3 normal vibration of the OCS molecule, and then used this surface to calculate the infrared spectra of the hydrogen-OCS complexes.[18]

In the present paper, we report a- and b-type rotational transitions in the ground vibrational state of all of the isotopic hydrogen-OCS complexes—p-H_2–OCS, o-H_2–OCS, HD–OCS, o-D_2–OCS, and p-D_2–OCS—by means of Fourier transform microwave (FTM) spectroscopy of a pulsed supersonic molecular beam. The experimental determination of the nuclear hyperfine structure due to the hydrogen unit and the corresponding quantitative analyses on the mass-

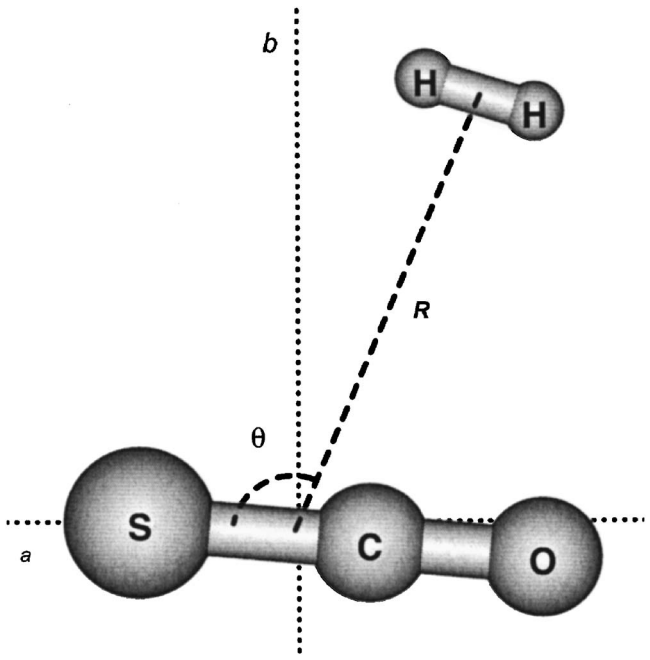

FIG. 1. The T-shaped molecular geometry of the hydrogen-OCS complexes in the ground state. R is the van der Waals bond distance and θ is the angle between the OCS axis and the $\boldsymbol{R}$ vector. Dotted lines indicate the orientation of the inertial axes for H_2–OCS.

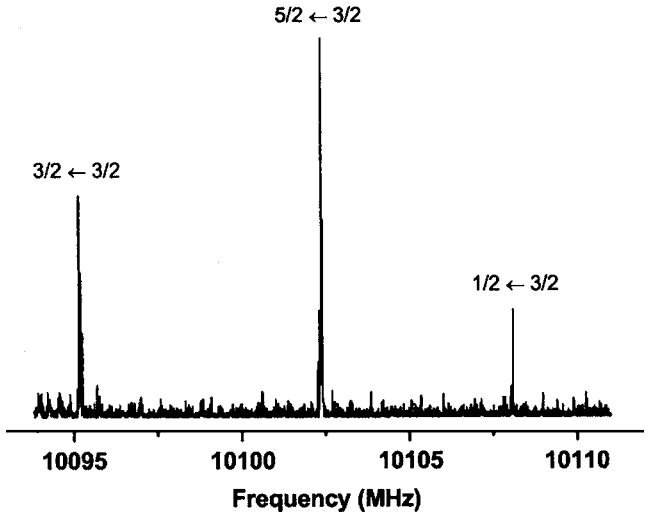

FIG. 2. The $1_{01} \leftarrow 0_{00}$ transition of o-H_2–$OC^{33}S$ showing well-resolved quadrupole hyperfine structure due to the $I_S=3/2$ ^{33}S nucleus. Lines are labeled by $F=J+I_S$ with the spin of the o-H_2 ignored. This is a composite of several scans to show all three hyperfine components.

dependent rotational dynamics have been reported.[15] We had interpreted the hyperfine structure in terms of a single component of angular momentum, $m_j=0$. Herein, we show that the $j=1$ hydrogen rotation is quenched and the ground rotational state for all five hydrogen-OCS species has total rotational angular momentum J equal to zero.

II. EXPERIMENTAL RESULTS

The experimental apparatus has been described in detail previously.[19,20] Briefly, hydrogen-OCS complexes are formed by pulsed supersonic expansion of a gas mixture of 0.2% OCS and 2%–10% hydrogen in either helium or neon through a pinhole nozzle of 1 mm diameter. Helium is used as the carrier gas for measurements of p-H_2–OCS, while neon is used for measurements of the other four species. Neon provides a better signal-to-noise ratio and a much narrower Doppler linewidth due to a lower beam velocity but cannot be used for p-H_2–OCS because of the stronger binding of Ne to OCS than p-H_2 to OCS. The stagnation pressure behind the pulsed valve is 3.5 atm, and the frequency of the FTM spectrometer is 6–42 GHz. Several a-type transitions for o-H_2–OCS, p-D_2–OCS, and o-D_2–OCS and their $OC^{34}S$ isotopomers were detected initially with a Fraser-type molecular beam electric resonance spectrometer,[21] but the spectral resolution was about one order of magnitude lower than with the FTM technique.

$\boldsymbol{J}$ is the total rotational angular momentum of the complex, $\boldsymbol{I}$ is the total nuclear spin angular momentum of the hydrogen unit, and $\boldsymbol{F}$ is the total angular momentum, $\boldsymbol{F}=\boldsymbol{J}+\boldsymbol{I}$. The hyperfine structure of the various $\boldsymbol{F}$ levels has been treated previously,[15] and the frequencies reported here are hyperfine-free line centers for transitions with resolvable hyperfine structure or the frequency of the most intense component for transitions without resolvable hyperfine structure.[22] The fundamental a- and b-type rotational transitions from the ground rotational state ($J=1 \leftarrow 0$) are observed for each complex, including both o-H_2–OCS and p-D_2–OCS, where $j=1$. These transitions originate in a $J=0$ state and confirm that the ground state for o-H_2–OCS and p-D_2–OCS has no contribution from the hydrogen rotational angular momentum.

The hydrogen was treated as a point mass, and the inertial system of hydrogen-OCS was assumed to be planar in the IR study.[17] Accordingly, the inertial a axis is nearly coincident with OCS (Fig. 1), and the b axis is close to the vector $\boldsymbol{R}$ connecting the centers of mass of OCS and hydrogen. Spectroscopic evidence supporting this inertial system is provided by the nuclear quadrupole coupling of ^{33}S ($I=3/2$) for o-H_2–$OC^{33}S$ in the $J_{K_aK_c}=1_{01} \leftarrow 0_{00}$ transition. As shown in Fig. 2, three well-resolved components are observed, and an analysis of the structure yields a coupling constant of $eqQ=-28.632(40)$ MHz, which is quite close to that of free $OC^{33}S$ (−29.130 MHz)—a confirmation that the OCS is nearly coincident with the a axis of the frame and that the angular momentum of hydrogen is quenched. If this was not the case, eqQ of ^{33}S for o-H_2–$OC^{33}S$ could be appreciably different from that of $OC^{33}S$ based on the P_2 projection of the nuclear quadrupole coupling tensor onto the a axis of the complex.

The 1:3 ratio of nuclear spin statistical weights of p-H_2 and o-H_2 and the stronger binding of o-H_2 van der Waals complexes make p-H_2 complexes difficult to form using normal H_2. The only pure rotational spectra of p-H_2 complexes reported prior to this work are those of p-H_2–CO (Ref. 23) and p-H_2–HCN (Ref. 24), which were measured only in the millimeter-wave spectral region, where a H_2 nuclear hyperfine structure is not resolved. We find experimentally that by carefully controlling the mole fraction of normal H_2 in the H_2/He gas mixture, the more weakly bound species He–OCS and p-H_2–OCS can be generated with an appreciable intensity, as shown in Fig. 3. These observations help explain

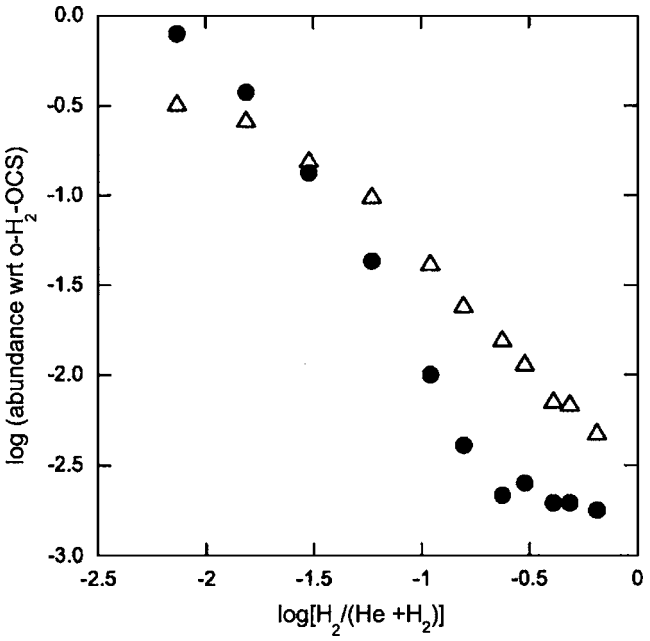

FIG. 3. Relative abundances of p-H_2–OCS (triangles) and He–OCS (filled circles) with respect to o-H_2–OCS in a pulsed supersonic expansion of 0.2% OCS seeded in a mixture of normal H_2 and He as a function of the partial pressure of normal H_2. The abundances are determined using the FTM signal intensities of the 2_{02}-1_{01} transition of each complex. The relative concentrations of p-H_2–OCS and He–OCS increase exponentially with decreasing H_2 component in the gas mixture.

why in previous spectroscopic studies where high percentages (>30%) of normal H_2 were used, such as H_2–HF,[25] H_2–OH,[26] and H_2–H_2O,[27] only o-H_2 forms of the complexes were observed. Furthermore, when neon is used instead of helium, the abundance of p-H_2–OCS decreases, while that of o-H_2–OCS increases, indicating that the binding energy of Ne–OCS is larger than p-H_2–OCS but lower than o-H_2–OCS.

Rotational transitions of hydrogen-OCS complexes with J up to 4 and K_a=0, 1 have been measured from 8 to 40 GHz and are listed in Table I. Higher K_a levels cannot be measured because of the large A rotational constants of the complexes and the low rotational temperature of the molecular beam. The measured transition frequencies for each complex, viewed as a nearly symmetric prolate rotor, can be readily fitted using Watson's A-reduced Hamiltonian[28]

$$H = \tfrac{1}{2}(B+C)J^2 + \left[A - \tfrac{1}{2}(B+C)\right]J_a^2 + \tfrac{1}{2}(B-C)(J_b^2 - J_c^2) - \Delta_J J^4 - \Delta_{JK} J_a^2 J^2 - \Delta_K J_a^4 - 2\delta_J J^2 (J_b^2 - J_c^2) - 2\delta_K [J_a^2 (J_b^2 - J_c^2) + (J_b^2 - J_c^2) J_a^2] + \Phi_{JK} J_a^2 J^4 + 2\phi_J J^4 (J_b^2 - J_c^2). \quad (1)$$

The spectroscopic parameters for the five hydrogen-OCS complexes determined using Pickett's SPFIT program[29] are listed in Table II. Like He–OCS, the large nonrigidity of hydrogen-OCS leads to large centrifugal distortion constants. At least eight adjustable parameters are required to fit the observations with fit residuals comparable to the measurement uncertainty. The lack of higher K_a transitions results in the indeterminability of higher order distortion constants involving J_a, such as Δ_K and δ_K, and therefore these constants were constrained in the fit to lie within 15% of preliminary predictions from calculations performed using an *ab initio* potential.[16] For the species with j=0, spectroscopic parameters of hydrogen-OCS complexes are essentially correlated linearly with the mass of the hydrogen unit. A, B, C, and Δ_{JK} decrease with increasing mass of the hydrogen unit while Δ_J and δ_J increase.

Nine a-type and four b-type rotational transitions of p-H_2–OCS are listed in Table I. These transitions are in good agreement with those predicted from the IR study, with the differences amounting to less than 3 MHz for the a-type transitions.[17] Even without the detection of b-type transitions, the IR study predicted A to be 22 805(240) MHz, within 2σ of our determination of 22 401.889(4) MHz. Our experimental results are also consistent with theoretical pre-

TABLE I. The observed transitions (in MHz) of the weakly bound hydrogen-OCS complexes. Maximum experimental uncertainty is estimated to be 5 kHz for p-H_2–OCS and 2 kHz for the other species. (The values in parentheses are obs.–calc. values in kHz.)

Transition	p-H_2–OCS	o-H_2–OCS	HD–OCS	o-D_2–OCS	p-D_2–OCS
2_{02}–1_{11}			9745.059(4)		10 758.476(–1)
3_{12}–3_{13}	8259.582(0)	6728.000(0)	9960.383(0)	10 874.893(0)	9689.052(0)
1_{01}–0_{00}	10 595.586(–1)	10 218.255(–1)	10 024.997(–1)	9517.559(7)	9289.155(0)
4_{13}–4_{14}	13 744.764(0)				
1_{10}–1_{01}	17 773.021(2)	18 378.973(3)	11 778.966(5)	8974.347(2)	9205.545(–1)
2_{11}–2_{02}	19 210.809(–1)	19 539.715(–2)	13 617.617(–3)	11 091.962(–2)	11 050.778(1)
3_{12}–3_{03}	21 519.761(–1)	21 381.849(1)	16 705.907(1)	14 766.151(2)	14 213.799(–1)
2_{12}–1_{11}	19 791.114(1)	19 304.742(–1)	18 373.767(5)	17 208.713(6)	16 954.572(–1)
2_{02}–1_{01}	21 108.051(1)	20 385.663(5)	19 860.567(–2)	18 728.250(–4)	18 845.878(1)
1_{11}–0_{00}	26 990.819(0)	27 477.568(–1)	20 140.510(–3)	16 672.205(–9)	16 876.557(1)
3_{03}–2_{12}			20 703.356(–8)		20 770.548(1)
2_{11}–1_{10}	22 545.842(1)	21 546.406(1)	21 699.224(–4)	20 845.863(–10)	20 191.109(1)
3_{13}–2_{12}	29 637.566(1)	28 926.751(–1)	27 448.881(–6)	25 634.365(–2)	25 295.297(2)
3_{03}–2_{02}	31 455.677(–3)	30 451.299(–4)	29 332.064(–7)	27 378.219(–7)	26 966.644(1)
3_{12}–2_{11}	33 764.633(1)	32 293.434(0)	32 420.357(0)	31 052.408(–5)	
4_{14}–3_{13}			36 406.770(–7)	33 886.883(–16)	33 498.754(3)
4_{04}–3_{03}			38 331.562(30)	35 410.020(45)	35 066.996(–10)

TABLE II. The determined spectroscopic constants (in MHz) of hydrogen-OCS complexes. (Numbers in parentheses represent one standard error in the fit.)

Constant	p-H_2–OCS	o-H_2–OCS	HD–OCS	o-D_2–OCS	p-D_2–OCS
A	22 401.889(4)	22 942.218(6)	15 970.010(3)	12 829.2875(9)	13 046.800(3)
B	5993.774(2)	5675.156(7)	5847.595(1)	5671.3573(7)	5454.612(2)
C	4602.038(2)	4542.960(7)	4177.699(1)	3846.7041(6)	3834.590(2)
Δ_J	0.056 35(6)	−0.034 82(8)	0.073 54(5)	0.125 68(2)	0.011 76(7)
Δ_{JK}	5.352(1)	2.934(2)	2.942(1)	1.2042(3)	1.288(1)
Δ_K[a]	[9.161]	[8.145]	[4.245]	[3.352]	[3.144]
δ_J	0.0177(1)	−0.0503(8)	0.0311(1)	0.047 08(5)	−0.0044(1)
δ_K[a]	[3.452]	[3.235]	[1.548]	[1.144]	[0.4778]
Φ_{JK}	0.001 98(9)	−0.0010(1)	0.000 75(7)	0.000 14(2)	−0.001 19(9)
ϕ_J	0.000 022(5)	−0.000 17(4)	0.000 108(6)	0.000 026(2)	0.000 060(7)
No. of transitions	13	12	16	14	15
rms	0.0022	0.0032	0.0038	0.0011	0.0068

[a]Constrained to lie within 15% of the preliminary *ab initio* value (Ref. 16).

dictions from bound state calculations using a four-dimensional potential energy surface of H_2–OCS, which will be presented elsewhere.[16] The absence of nuclear spin-spin splitting in the $1_{01} \leftarrow 0_{00}$ transition confirms that the detected species contains p-H_2 ($I=0$). Because the b component of the transition dipole moment of p-H_2–OCS has been predicted previously to be about 1/50 of the a component,[17] a p-H_2 enriched sample rather than normal H_2 was used to detect the b-type transitions.

The rotational spectrum of o-H_2–OCS is very similar to that of p-H_2–OCS, in accord with quenching of the o-H_2 $j=1$ angular momentum. The A rotational constant of o-H_2–OCS is 2.4% greater than that of p-H_2–OCS, while the B and C constants are 5.3% and 1.3% smaller, respectively. As with p-H_2–OCS, a-type transitions are within 3 MHz of the IR predictions, but, in contrast, the A value from the IR study is ~300 MHz lower than our determination while for p-H_2–OCS the A value from the IR study is ~400 MHz *higher* than our determination. The centrifugal distortion constants are all lower than those of p-H_2–OCS, with four negative in sign. These nonphysical distortion constants may arise because of interactions with the low-lying orientational states; the only other species with similarly negative distortion constants is p-D_2–OCS, which also has the two additional low-lying orientational states.

Both o-D_2–OCS and p-D_2–OCS are readily formed using normal D_2. As before, when neon is used instead of helium as the carrier gas, the signal-to-noise ratio is improved by at least one order of magnitude, an indicator that the binding energies of o-D_2–OCS and p-D_2–OCS are larger than Ne–OCS. Fourteen a- and b-type transitions of o-D_2–OCS have been measured (Table I), and all of these, even the b-type transitions, are within a few megahertz of the predictions based on the IR study. The A rotational constant of o-D_2–OCS is nearly half that of p-H_2–OCS in accordance with its T-shaped structure. Although o-D_2–OCS should be more rigid than p-H_2–OCS due to its larger binding energy, it is difficult to draw this conclusion on the basis of the derived centrifugal distortion constants. Four of the o-D_2–OCS constants, including the two estimated from calculations, are smaller than those of p-H_2–OCS, two are larger, and one is essentially the same.

It is worthwhile to compare He–OCS and o-D_2–OCS because of their similarity in mass and structure. In principle, o-D_2 should be similar to atomic helium, but comparing the rotational constants of o-D_2–OCS and He–OCS (Ref. 30) reveals several key differences, particularly with respect to the amplitudes of the radial and angular zero-point oscillations, which are larger for He–OCS. The B and C rotational constants of o-D_2–OCS are larger by 3.0% and 5.1%, respectively, than those of He–OCS, as expected, but A is smaller by about 2.9%. Centrifugal distortion constants of o-D_2–OCS are significantly smaller than those of He–OCS, except for Δ_{JK}. For example, $\Delta_J=0.9406(6)$ MHz and $\delta_J=0.336\,60(6)$ MHz for He–OCS, compared to $\Delta_J=0.125\,68(2)$ MHz and $\delta_J=0.047\,08(5)$ MHz for o-D_2–OCS. This is in agreement with a stronger intermolecular interaction and larger anisotropy for o-D_2–OCS.

The rotational spectra of p-D_2–OCS, in which $j=1$ and $I=1$, appears similar to o-D_2–OCS, as expected from the discussion of p-H_2–OCS and o-H_2–OCS. Fifteen a- and b-type rotational transitions (Table I) have been measured, and the best-fit spectroscopic constants are summarized in Table II; derived constants and fit residuals are similar to those found for o-D_2–OCS. Five of the seven centrifugal distortion constants for p-D_2–OCS are smaller than the corresponding constants of o-D_2–OCS, with two negative in sign. Although p-D_2–OCS is more tightly bound than o-D_2–OCS, it is difficult to draw definitive conclusions based on a comparison of distortion constants without fully accounting for Coriolis interactions with the low-lying orientational states of p-D_2–OCS.

HD provides another $j=0$ hydrogen species in the low-temperature molecular beam. Sixteen a- and b-type transitions of HD–OCS have been observed and are listed in Table I. Best-fit spectroscopic constants for HD–OCS derived from Watson's Hamiltonian are listed in Table II; all are very close to the averaged value between p-H_2–OCS and o-D_2–OCS. For instance, $B=5847.595(1)$ MHz and $C=4177.699(1)$ MHz for HD–OCS, while the averages for p-H_2–OCS and o-D_2–OCS are 5832.566 MHz and 4224.371 MHz. The centrifugal distortion constants also lie between those of p-H_2–OCS and o-D_2–OCS, thus showing the simple scaling with the mass of spherical hydrogen.

III. DISCUSSION

An analysis of the relative abundances of H_2 and He complexes as a function of the H_2/He ratio (Fig. 3) suggests that binding energies decrease from o-H_2–OCS to He–OCS. This relative ordering is consistent with theoretical predictions from an *ab initio* intermolecular potential energy surface and bound state calculation.[16] The energy splitting between the free-space m_j levels for $j=1$ o-H_2–OCS resulting from the anisotropy of the intermolecular interaction pushes the lower A' bound state below that of the ground state of the p-H_2–OCS complex. This anisotropic coupling assures that o-H_2 complexes in the ground state always have a larger dissociation energy than the p-H_2 complexes. For this reason, weakly bound p-H_2 complexes have been very difficult to detect using normal H_2 as the precursor. The same argument is applicable to D_2, where o-D_2 species will have lower binding energies than p-D_2 species; however, the nuclear spin weight of 6 for o-D_2 compared to 3 for p-D_2 gives o-D_2 an abundance advantage that p-H_2 does not share. We have demonstrated in this study that under optimized conditions, the generation of weakly bound p-H_2 complexes can be achieved using normal hydrogen. From the relative line intensities we infer that binding energies of weakly bound OCS complexes are, in order,

$$\text{He}-\text{OCS} < \text{p-H}_2-\text{OCS} < \text{Ne}-\text{OCS} < \text{o-H}_2-\text{OCS} < \text{HD}-\text{OCS} < \text{o-D}_2-\text{OCS} < \text{p-D}_2-\text{OCS}.$$

The delicacy of this ordering shows the important role of zero-point energy for weakly bound van der Waals complexes.

Although the spectra and fitted constants are similar for the $j=0$ and 1 species, it is instructive to compare inertial defects between them. For the nearly planar complexes discussed here the inertial defect can be described as

$$\Delta = I_c^\circ - I_a^\circ - I_b^\circ + 2P_c, \tag{2}$$

where I_x° is the moment of inertia in the ground vibrational state with respect to the x axis and P_c is the second moment of the c axis due to the slight out-of-plane distribution of the hydrogens. The inertial defects for the $j=0$ species, p-H_2–OCS, HD–OCS, and o-D_2–OCS, are 3.137, 3.196, and 3.271 amu Å^2, respectively, in contrast to those for the $j=1$ species which are 0.283 amu Å^2 for o-H_2–OCS and 0.644 amu Å^2 for p-D_2–OCS. For comparison, the inertial defect of He–OCS is 7.950 amu Å^2.[30] Table III lists inertial defects and structural parameters of these and other atom-OCS complexes.[31–35] The inertial defect is composed of contributions from vibration Δ_{vib}, centrifugal distortion Δ_{cent} and electron-rotation interaction Δ_{elec},[36] with Δ_{vib} and Δ_{cent} as the dominant terms for weakly bound complexes. The large disparity in inertial defect between the $j=0$ and 1 species is most likely due to the interaction between the ground state and the low-lying orientational states for the $j=1$ species. Symmetry considerations dictate that Coriolis interactions occur between the A' ground state and the first excited orientational state, which is A'' symmetry, through rotation about the inertial a and b axes, while Coriolis interactions with the second excited orientational state and the van der Waals bending state, which are both A' symmetry, occur through rotation about the c inertial axis.[37] These interactions serve to lower the apparent rotational constant associated with the axis and thus affect the inertial defect. The interaction with the A'' state should be greatest since it is closer energetically, and this will lower the inertial defect compared to those of the $j=0$ species.

TABLE III. A comparison of structural parameters of atom-OCS complexes determined using the method described in the text. Numbers in parentheses are literature values determined using the A and C rotational constants.

Complex	Δ (amu Å^2)	R (Å)	θ (°)
p-H_2–OCS	3.137	3.69	103.0
HD–OCS	3.196	3.61	104.9
o-D_2–OCS	3.271	3.56	105.7
o-H_2–OCS	0.283	[3.78][a]	[113.0][a]
p-D_2–OCS	0.644	[3.57][a]	[108.8][a]
He–OCS[b]	7.950	3.82	109.2
^{20}Ne–OCS[c]	4.365	3.54(3.535)	108.2(109.58)
Ar–OCS[d]	2.827	3.70(3.701)	105.4(106.7)
^{84}Kr–OCS[e]	2.585	3.81(3.806)	104.5(105.9)
^{202}Hg–OCS[f]	2.488	3.77(3.769)	100.1(101.7)

[a]As discussed in the text, structural parameters for $j=1$ species are simply presented for comparison.
[b]Reference 30.
[c]Reference 33.
[d]Derived from rotational constants in Ref. 34 that were fit to data from Refs. 31 and 32.
[e]Reference 34.
[f]Reference 35.

The inertial defect of the $j=0$ species can be used to predict the van der Waals bending frequency using a formula from Herschbach and Laurie,[38]

$$\Delta_{\text{vib}} = 4K/\omega_b, \tag{3}$$

where $K=h/8\pi^2c=16.8576$ amu Å^2/cm and ω_b is the frequency (in cm^{-1}) of the lowest bending state. While this simple formula was developed with strongly bound molecules in mind, it does remarkably well for predicting the lowest lying bending vibration of atom-OCS complexes. To our knowledge, no soft-mode bending frequencies have been measured experimentally for atom-OCS complexes, so we must rely on recent high-level computational studies to demonstrate this point. Xie and co-workers have performed calculations on Ne–OCS (Ref. 39) and Ar–OCS (Ref. 40) using an *ab initio* potential to predict bound state energies and ground state rotational and distortion constants, and using their data and known formulas to calculate Δ_{cent} from distortion constants,[36,41] we can obtain Δ_{vib} and thus predict ω_b from Eq. (3) for comparison with the calculated energy of the lowest lying bending level. For ^{20}Ne–OCS, Eq. (3) predicts $\omega_b=15.4$ cm^{-1} compared to 15.4 cm^{-1} for the calculated bending level, and for Ar–OCS, Eq. (3) predicts $\omega_b=24.6$ cm^{-1} compared to 24.3 cm^{-1} for the calculated bending level. Applying Eq. (3) to the $j=0$ species, which behave like atom-OCS complexes, yields bending frequencies of 24.2, 22.5, and 21.8 cm^{-1} for p-H_2–OCS, HD–OCS, and o-D_2–OCS, respectively. These frequencies are not simply related by the square root of the hydrogen unit's mass, an

indication of the interplay between mass, zero-point motion, and binding energy for these complexes.

The discussion of the geometry of hydrogen-OCS based on the rotational constants of the five species can only be approximate since we do not estimate the magnitude of the Coriolis interactions with the low-lying states for either the $j=0$ species, which will couple with the van der Waals bending state, or the $j=1$ species, which will couple with the two orientational states in addition to the van der Waals bending state. To estimate the structures of the various hydrogen-OCS species the hydrogen can be treated as a point mass and thus the complexes as semirigid atom-linear-molecule systems.[42] The two independent structural parameters, R and θ (as shown in Fig. 1), can be determined using two of the three rotational constants. The pairwise combinations A,C and B,C give the same value of R, but this value differs by as much as 0.2 Å from the value determined using the A,B combination. In addition, the three pairwise combinations give θ values that differ by as much as 10° from each other. In deciding which combination to use we are aided once again by previous *ab initio* calculations on atom-OCS complexes, in which $\langle R\rangle$, $\langle\theta\rangle$, and calculated rotational constants are presented.[30,39,40] Examining HeOCS, NeOCS, and ArOCS shows that R values determined using A,C or B,C are within ~0.01 Å of $\langle R\rangle$, while taking the *average* of the three θ values gives the best estimate of $\langle\theta\rangle$, lying within 0.1° for NeOCS and ArOCS and within 0.5° for HeOCS. Thus, we use A,C or B,C to determine R, and the average from the three combinations to determine θ. From this simplified model, we find for the $j=0$ species that R and θ vary monotonically with hydrogen mass with $R=3.69$, 3.61, and 3.56 Å and $\theta=103.0°$, 104.9°, and 105.7° for p-H_2–OCS, HD–OCS, and o-D_2–OCS, respectively. The $j=1$ species are heavily influenced by Coriolis interactions with the aforementioned low-lying orientational states, which leads to an apparent value of R for o-H_2–OCS of 3.78 Å, much larger than for the more weakly bound p-H_2–OCS species and, most likely, much larger than the true distance. Intuitively, the distance should be shorter than for p-H_2–OCS, and thus a determination based solely on measured effective rotational constants overestimates the distance for o-H_2–OCS by at least 0.1 Å. An accurate determination of the true distances for the $j=1$ species requires deperturbation of the rotational constants to remove the Coriolis influences, and this, in turn, requires knowledge of the low-lying interacting states and is beyond the scope of the current paper. The determined structural parameters for the hydrogen-OCS complexes as well as for other atom-OCS complexes are listed in Table III. These OCS complexes vary significantly in their binding energies, but their molecular structures are surprisingly similar to each other with respect to the magnitude of R and θ. From our results the angle between OCS and the a-inertial axis is estimated to be 5.6°, 10.1°, and 15.3° and the a/b transition dipole moment ratio to be 10.3, 5.6, and 3.7 for p-H_2–OCS, HD–OCS, and o-D_2–OCS, respectively. However, since the transition intensity measured in this study is very sensitive to the mode quality of the Fabry-Pérot cavity, we are unable to quantitatively determine the intensity ratio between a- and b-type transitions of the hydrogen-OCS complexes.

IV. CONCLUSION

Our understanding of binary complexes formed with hydrogen has been changed considerably in the course of this study. The inability to readily form complexes of p-H_2 using normal H_2 is the result of using too much H_2, a problem easily solved when using He as the carrier gas. Since the binding energy of o-H_2 is generally greater than that of p-H_2, while that of He is less than p-H_2, optimal gas mixtures are relatively easy to determine. In this sense the reactivity of normal H_2 should be taken into account. The surprising simplicity of the spectra of the $j=1$ hydrogen complexes, o-H_2 and p-D_2, was greatly clarified when the point group symmetry of the complex was considered. In particular, the discovery that these species have $J=0$ ground states rather than $J=1$, as might be expected based on simple angular momentum coupling arguments, became clear.

The large energy difference between allowed rotational levels of hydrogen provides insight into weakly bound hydrogen complexes by limiting the mixing of higher j states into the ground and other low-lying states. The hydrogen submolecule wave functions are the single spherical function for the three $j=0$ species and the three Cartesian vector functions for the $j=1$ species o-H_2 and p-D_2. For hydrogen-OCS the three hydrogen orientations have different energies. The present study deals only with the ground orientational state of these complexes. The description of the ground orientational level is best found by means of the hyperfine structure and is completely compatible with the hydrogen orientation lying in the symmetry plane and essentially parallel to the OCS axis.[15]

A complete understanding of the $j=1$ species requires knowledge of the unobserved low-lying orientational states and their influence on the ground state. While it may be possible to obtain this knowledge experimentally, and, in fact, we have several unassigned lines that could be rotational transitions of one or more of the orientational states, the observation of the low-lying orientational states will likely be difficult given the estimated ~20 cm^{-1} excitation energy of the first orientational state and the low temperature of the beam. Recent observations of a high energy polar form of OCS dimer in a helium expansion give hope.[43] A more fruitful approach supplements experiment with computation and is currently underway. This may allow an adequate estimation of the Coriolis interactions observable in the present spectroscopic constants and, in turn, calculation of realistic structural parameters for the $j=1$ species.

ACKNOWLEDGMENTS

We are indebted to Dr. A. R. W. McKellar for generously providing us the enriched para-H_2 sample and helpful discussions. We would also like to thank E. S. Palmer for invaluable laboratory support. This work is financially supported by the Chemical Division of the National Science Foundation under Grant Nos. CHE-0138531 and CHE-0353693 and by the Petroleum Research Fund of the American Chemical Society.

[1] S. Grebenev, B. G. Sartakov, J. P. Toennies, and A. F. Vilesov, Science **289**, 1532 (2000).
[2] S. Grebenev, B. G. Sartakov, J. P. Toennies, and A. F. Vilesov, J. Chem. Phys. **114**, 617 (2001).
[3] S. Grebenev, B. Sartakov, J. P. Toennies, and A. Vilesov, Phys. Rev. Lett. **89**, 225301 (2002).
[4] R. Fröchtenicht, J. P. Toennies, and A. Vilesov, Chem. Phys. Lett. **229**, 1 (1994).
[5] M. Hartmann, R. E. Miller, J. P. Toennies, and A. Vilesov, Phys. Rev. Lett. **75**, 1566 (1995).
[6] M. Hartmann, R. E. Miller, J. P. Toennies, and A. Vilesov, Science **272**, 1631 (1996).
[7] S. Goyal, D. L. Schutt, and G. Scoles, Phys. Rev. Lett. **69**, 933 (1992).
[8] J. Higgins, W. E. Ernst, C. Callegari, J. Reho, K. K. Lehmann, G. Scoles, and M. Gutowski, Phys. Rev. Lett. **77**, 4532 (1996).
[9] Y. Kwon and K. B. Whaley, Phys. Rev. Lett. **89**, 273401 (2002).
[10] F. Paesani, R. E. Zillich, and K. B. Whaley, J. Chem. Phys. **119**, 11682 (2003).
[11] D. T. Moore and R. E. Miller, J. Chem. Phys. **119**, 4713 (2003).
[12] Y. Kwon and K. B. Whaley, Phys. Rev. Lett. **89**, 273401 (2002).
[13] I. F. Silvera, Rev. Mod. Phys. **52**, 393 (1980).
[14] P. Jankowski and K. Szalewicz, J. Chem. Phys. **123**, 104301 (2005).
[15] Z. Yu, K. J. Higgins, W. Klemperer, M. C. McCarthy, and P. Thaddeus, J. Chem. Phys. **123**, 221106 (2005).
[16] K. J. Higgins, Z. Yu, and W. Klemperer, 57th Ohio State University International Symposium on Molecular Spectroscopy, Columbus, OH, June 17–21, 2002 (unpublished), Paper RA02; K. J. Higgins, Z. Yu, and W. Klemperer, 62nd Ohio State University International Symposium on Molecular Spectroscopy, Columbus, OH, June 18–22, 2007 (unpublished), Paper FB10.
[17] J. Tang and A. R. W. McKellar, J. Chem. Phys. **116**, 646 (2002).
[18] F. Paesani and K. B. Whaley, Mol. Phys. **104**, 61 (2006).
[19] T. J. Balle and W. H. Flygare, Rev. Sci. Instrum. **52**, 33 (1981).
[20] M. C. McCarthy, M. J. Travers, A. Kovacs, C. A. Gottlieb, and P. Thaddeus, Astrophys. J., Suppl. Ser. **113**, 105 (1997).
[21] S. Drucker, A. L. Cooksy, and W. Klemperer, J. Chem. Phys. **98**, 5158 (1993).
[22] Typically, the $J=1\leftarrow 0$ transitions have resolvable hyperfine structure. For other transitions the strongest component is the center component, and this differs from the hyperfine free line center only by several kilohertz, which is better than the resolution of the spectrometer.
[23] I. Pak, L. A. Surin, B. S. Dumesh, D. A. Roth, F. Lewen, and G. Winnewisser, Chem. Phys. Lett. **304**, 145 (1999).
[24] M. Ishiguro, T. Tanaka, K. Harada, W. Kensuke, J. W. Christopher, and K. Tanaka, J. Chem. Phys. **115**, 5155 (2001).
[25] C. M. Lovejoy, D. D. Nelson, Jr., and D. J. Nesbitt, J. Chem. Phys. **87**, 5621 (1987).
[26] M. D. Wheeler, M. W. Todd, D. T. Anderson, and M. I. Lester, J. Chem. Phys. **110**, 6732 (1999).
[27] M. J. Weida and D. J. Nesbitt, J. Chem. Phys. **110**, 156 (1999).
[28] J. K. G. Watson, J. Chem. Phys. **46**, 1935 (1967).
[29] H. M. Pickett, J. Mol. Spectrosc. **148**, 371 (1991).
[30] K. Higgins and W. Klemperer, J. Chem. Phys. **110**, 1383 (1999).
[31] S. J. Harris, K. C. Janda, S. E. Novick, and W. Klemperer, J. Chem. Phys. **63**, 881 (1975).
[32] J. A. Shea, W. G. Read, and E. J. Campbell, J. Chem. Phys. **79**, 2559 (1983).
[33] Y. Xu and M. C. L. Gerry, J. Mol. Spectrosc. **169**, 542 (1995).
[34] F. J. Lovas and R. D. Suenram, J. Chem. Phys. **87**, 2010 (1987).
[35] M. Iida, Y. Ohshima, and Y. Endo, J. Chem. Phys. **94**, 6989 (1991).
[36] T. Oka and Y. Morino, J. Mol. Spectrosc. **6**, 472 (1961).
[37] H. A. Jahn, Phys. Rev. **56**, 680 (1939).
[38] D. R. Herschbach and V. W. Laurie, J. Chem. Phys. **40**, 3142 (1964).
[39] H. Zhu, Y. Zhou, and D. Xie, J. Chem. Phys. **122**, 234312 (2005).
[40] H. Zhu, Y. Guo, Y. Xue, and D. Xie, J. Comput. Chem. **27**, 1045 (2006).
[41] W. Gordy and R. L. Cook, in *Microwave Molecular Spectra* (Wiley, New York, 1984).
[42] G. D. Hayman, J. Hodge, B. J. Howard, J. S. Muenter, and T. R. Dyke, J. Mol. Spectrosc. **133**, 423 (1989).
[43] M. Afshari, M. Dehghani, Z. Abusara, N. Moazzen-Ahmadi, and A. R. W. McKellar, J. Chem. Phys. **126**, 071102 (2007); A. J. Minei and S. E. Novick, *ibid.* **126**, 101101 (2007).